DOE/ET-53088-208 IFSR #208

STUDY OF THE MAGNETIC COMPRESSIONAL MODE IN A HOT PARTICLE PLASMA

D.P. Stotler, H.L. Berk, and M.G. Engquist
Institute for Fusion Studies
The University of Texas at Austin
Austin, Texas 78712

September 1985

Study of the Magnetic Compressional Mode in a Hot Particle Plasma

D.P. Stotler, H.L. Berk, and *M.G. Engquist*

Institute for Fusion Studies

The University of Texas at Austin

Austin, Texas 78712

Abstract

The integral equation for the magnetic compressional mode, accounting for geometrical effects along the field line and using the eikonal approximation across the field line, is solved numerically for the eigenvalues and eigenfunctions. These results reproduce the analytic estimates when there is strong drift reversal. The representation of the eigenfunction of the form $\hat{B}_{||} = \left(C(\psi)/B\right)\frac{dP_{\perp h}}{d\psi}$ is found to give accurate growth rates over a large range of parameter values. For typical EBT-S parameters, instability is observed for all pressure scale lengths just below those needed for drift reversal, i.e. $|R\partial(P_c + P_{\perp h})/2B^2\partial r| > 1$ (where P is the particle pressure, c and h refer to cold and hot components, B is the midplane magnetic field, and R is the midplane radius of curvature). If larger core densities are present, a wave-particle resonance arises when the particle drifts are not reversed, causing instability up to much larger pressure scale lengths. Stability for all values of the ratio of hot electron density to core density is obtained with $|R\partial P_c/B^2\partial r| > 1 + P_{||h}/P_{\perp h}$.

I. Introduction

Systems in which the magnetic drift frequencies are large compared to those encountered in magnetohydrodynamic (MHD) theory may be susceptible to a magnetic compressional instability. In particular, this would be the case if one attempted to stabilize otherwise MHD unstable systems by introducing a super-hot component.[1,2,3] The example which we will study here is of the trapped particles forming the hot electron rings in the Elmo Bumpy Torus (EBT) device. This mode is also of great interest in symmetric tandem mirrors employing a super-hot component in a similar role. In either case, it is hoped that the system is stabilized by the minimum-B of the diamagnetic well formed by the anisotropic pressure of these energetic particles, which are trapped in regions of unfavorable curvature. However, the reversal of the vacuum grad-B in the bad curvature areas can lead to a magnetic instability having the polarization of a compressional Alfvén wave, i.e., with the perturbed magnetic field, $\hat{\mathbf{B}}_{||} \parallel \mathbf{B}_0$. In EBT such a mode can arise if the background density is too high. This mode is just one aspect of the hot particle stability picture; even if this mode is stable, the system may still be susceptible to MHD-like instabilities, such as the interacting pressure-driven interchange mode,[2] and precessional modes.[4,5]

Here, we consider the numerical solution of the integral equation describing this mode for a single cell of an axisymmetric multi-mirror system. In general, a pair of coupled equations involving $\hat{B}_{||}$, the perturbed magnetic field, and $\hat{\varphi}$, the perturbed electrostatic potential, must be solved simultaneously. Due to the large difference in frequency between the magnetic compressional mode and the interchange mode arising out of the $\hat{\varphi}$ equation, we do not expect this coupling to strongly affect the magnetic compressional mode. Thus, we solve here only one equation in $\hat{B}_{||}$, and will study the coupled system in subsequent work. The integral equation arises from the high bounce frequency of the trapped hot electrons. We assume that the perturbation has an eikonal behavior in the direction perpendicular to $\mathbf{B}_0$. A relatively simple solution arises in a deep diamagnetic well. However, for a moderate well, the simple solution is unjustified and a numerical solution of the integral equation is necessary. We find that more pessimistic results arise than from the simple theory. Study of the solutions leads one to believe that a description of the mode with the

assumption that $\hat{B}_{||} = \big(C(\psi)/B\big)dP_{\perp h}/d\psi$ is accurate for growth rates if the subsequent integrals are not approximated further.

In Sec. II, the numerical model is developed from the governing equations. Section III presents some eigenvalues and eigenfunctions obtained from its solution. Finally, a summary of these results is given in Sec. IV.

II. Numerical Model

The general equations describing the response of a plasma containing a highly energetic species to a perturbation of arbitrary polarization in a multi-cell, bumpy cylinder geometry have been derived elsewhere.[6,7] Treating the hot electrons with a drift-kinetic description, and employing an MHD response for the core plasma, these equations retain finite Larmor radius (FLR) effects and allow frequencies comparable to the ion cyclotron frequency. Here, we seek a much simpler system to solve and neglect the FLR terms, as well as taking the limit $\omega/\omega_b << 1$; ω_b is the hot electron bounce frequency. The resulting equation describes the perturbed parallel magnetic field when written in the form

$$B_{||}(\mathbf{x}) = \hat{B}_{||}(s)\exp[iS(\psi,\theta)],$$

with $\mathbf{k}_\perp = \frac{\ell}{r}\hat{\theta} + \nabla\psi\frac{\partial S}{\partial\psi}$. We find that the amplitude satisfies

$$\hat{B}_{||}\left(1+\frac{1}{B}\,\frac{\partial P_{\perp h}}{\partial B}\Big|_\psi + \beta_c - \frac{\omega^2}{k_\perp^2 v_A^2}\right)$$
$$= m_h\int\frac{d\epsilon d\mu B}{|v_{||}|}\mu^2\left[\frac{\omega\frac{\partial F_h}{\partial\epsilon}(\epsilon,\mu,\psi)+\frac{m_h\ell}{q_h}\frac{\partial F_h}{\partial\psi}}{\omega-\langle\omega_d\rangle}\right]\langle\hat{B}_{||}\rangle, \qquad (1)$$

where

$$\langle\omega_d\rangle = \frac{\ell m_h}{q_h}\left[\mu\left\langle\frac{dB}{d\psi}\right\rangle + \left\langle\frac{v_{||}^2\kappa}{rB}\right\rangle\right] \equiv \langle\omega_{bh}\rangle + \langle\omega_{\kappa h}\rangle$$

$$\langle\alpha\rangle = \oint\frac{ds}{|v_{||}|}\alpha\Big/\oint\frac{ds}{|v_{||}|}$$

$$|v_{||}| = \sqrt{2}[\epsilon-\mu B(s,\psi)]^{1/2} \quad , \quad \mu = v_\perp^2/2B$$

$$\kappa = |(\hat{b}\cdot\nabla)\hat{b}|$$

$$P_{\perp h} = m_h \int \frac{d\epsilon d\mu B^2}{|v_{||}|} \mu F_h(\epsilon, \mu, \psi)$$

$$k_\perp^2 = \frac{\ell^2}{r^2} + \left(\frac{\partial S}{\partial \psi}\right)^2 |\nabla\psi|^2$$

$$\nabla\psi \times \hat{\theta} = r\mathbf{B}$$

$$\frac{d}{d\psi} \equiv \frac{\nabla\psi \cdot \nabla}{|\nabla\psi|^2} \equiv \frac{\partial}{\partial\psi}\bigg|_B + \frac{dB}{d\psi}\frac{\partial}{\partial B}\bigg|_\psi$$

$$\beta_c = 2P_c/B^2.$$

m_i and q_i are the particle mass and charge, respectively. The subscripts h and c then refer to the hot and background species. Note that the core plasma is assumed to be isotropic.

In the limit that $|(1/B)\partial P_{\perp h}/\partial\psi| >> |\kappa/r|$, this equation can be readily solved. In fact, to lowest order in κ, it can be shown[6] that $\hat{B}_{||} \cong \big(C(\psi)/B\big) dP_{\perp h}/d\psi$. Expanding the resonant denominator of Eq. (1) with $\omega << \omega_{bh}$, $\omega_{\kappa h}$ leads to a dispersion relation,

$$\int_0^{L/2} \frac{ds}{B}\left[\frac{dP_{\perp h}}{d\psi}\frac{d}{d\psi}\left(\frac{P_c}{B^2}\right) + \frac{q_h\omega_B}{\ell}\frac{d}{d\psi}\left(\frac{n_h}{B}\right) - \frac{\kappa}{rB}\frac{d}{d\psi}(P_{\perp h} + P_{||h})\right.$$
$$\left. - \frac{\omega^2}{k_\perp^2 v_A^2}\left(\frac{1}{B}\frac{dP_{\perp h}}{d\psi}\right)^2\right] = 0. \qquad (2)$$

The integral is carried out from the midplane of the cell to the mirror throat.

Of course, when $|1/BdP_{\perp h}/d\psi| \cong |\kappa/r|$, this solution is inappropriate and we must solve the equation numerically. For this purpose, we expand $\hat{B}_{||}$ in a complete set of functions, f_n, of s, the length along a field line from midplane,

$$\hat{B}_{||}(s) = \sum_{n=1}^{\infty} a_n f_n(s).$$

The solution yields a value for ω and gives the constant coefficients, a_n.

When there is no coupling to the perturbed electrostatic potential, as is the case here, $\hat{B}_{||}$ vanishes outside of the hot electron region. We assume $\hat{B}_{||}$ to be even in s; the symmetry of the system allows eigenfunctions which are even or odd. Then, it is reasonable to choose even functions which go through zero at the edge of the annulus and vanish outside of it:

$$f_n(s) = \begin{cases} \cos\left[\pi\frac{(n-1/2)s}{s_c}\right] & 0 \le s \le s_c \\ 0 & s_c \le s \le L, \end{cases} \qquad (3)$$

where $B(s_c) = B_c$. For comparison purposes, two other representations of $\hat{B}_{||}$ are investigated. The single term representation,

$$\hat{B}_{||} = a_0 \frac{1}{B} \frac{dP_{\perp h}}{d\psi},$$

is clearly valid when $\omega/\langle\omega_d\rangle << 1$, since $\hat{B}_{||} \cong \big(C(\psi)/B\big) dP_{\perp h}/d\psi$ in that case. We will assess the accuracy of this approach for larger values of $\omega/\langle\omega_d\rangle$.

Also, a Gaussian test function,

$$\hat{B}_{||} = \exp\left[-\frac{(s-s_0)^2}{\Delta_S^2}\right] + \exp\left[\frac{-(s+s_0)^2}{\Delta_S^2}\right] \tag{4}$$

will be employed. s_0 is fixed and Δ_S, a complex number in general, is varied so as to minimize the quadratic form.

In order to obtain the eigenvalue, ω, we first multiply Eq. (1) by $\hat{B}_{||}/B(s)$ and integrate along the field line. Using the above expansion for $\hat{B}_{||}$, we then have

$$\sum_{k,j=1}^{\infty} a_k a_j Q_{kj}(\omega) = 0,$$

where

$$Q_{kj}(\omega) = \int_0^{L/2} \frac{ds}{B}\left[f_k(s) f_j(s)\left(1 + \frac{1}{B}\frac{\partial P_{\perp h}}{\partial B}\Big|_{\psi} + \beta_c - \frac{\omega^2}{k_\perp^2 v_A^2}\right)\right]$$

$$- m_h \int_0^{L/2} \frac{ds}{B} \int \frac{d\epsilon d\mu}{|v_{||}|} \mu^2 B \frac{\left(\omega \frac{\partial F_h}{\partial \epsilon} + \frac{m_h \ell}{q_h}\frac{\partial F_h}{\partial \psi}\right)}{\omega - \langle\omega_d\rangle} \langle f_k\rangle\langle f_j\rangle.$$

Varying this expression with respect to a_i, we find

$$\sum_{j=1}^{\infty} a_j Q_{ij}(\omega) = 0,$$

for $i = 1, \infty$. Then, ω is determined by requiring that these equations have a non-trivial solution. That is,

$$\det\left|Q_{ij}(\omega)\right| = 0. \tag{5}$$

Specifically, we take

$$F_h = \begin{cases} \frac{4\hat{P}_{\perp h}}{m_h\sqrt{2\pi T^{7/2}}} \frac{\left[1 - \frac{(\psi-\psi_0)^2}{\Delta\psi^2}\right](\mu B_c - \epsilon)e^{-\epsilon/T}}{(1 - B_{\min}/B_c)^{3/2}(1 + 4B_c/B_{\min})} & \frac{\epsilon}{B_c} < \mu < \frac{\epsilon}{B_{\min}} \\ 0 & 0 < \mu < \frac{\epsilon}{B_c} \end{cases} \tag{6}$$

where $B_{\min} \equiv \min[B(s)] < B_c < B_{\max} \equiv \max[B(s)]$. Doing the appropriate integrals, the hot electron density and pressure can be obtained:

$$n_h = \frac{2\hat{P}_{\perp h}\left[1 - \frac{(\psi-\psi_0)^2}{\Delta\psi^2}\right]}{m_h T} \frac{B_c}{B} \frac{(1 - B/B_c)^{3/2}}{(1 - B_{\min}/B_c)^{3/2}(1 + 4B_c/B_{\min})}$$

$$\frac{1}{B}\frac{\partial n_h}{\partial B} = \frac{-2\hat{P}_{\perp h}}{m_h T}\left[1 - \frac{(\psi-\psi_0)^2}{\Delta\psi^2}\right] \frac{B_c}{B^3} \frac{(1 - B/B_c)^{1/2}(1 + \frac{1}{2}B/B_c)}{(1 - B_{\min}/B_c)^{3/2}(1 + 4B_c/B_{\min})}$$

$$P_{\perp h} = \hat{P}_{\perp h}\left[1 - \frac{(\psi-\psi_0)^2}{\Delta\psi^2}\right] \frac{(1 - B/B_c)^{3/2}(1 + 4B_c/B)}{(1 - B_{\min}/B_c)^{3/2}(1 + 4B_c/B_{\min})}$$

$$P_{\| h} = 2\hat{P}_{\perp h}\left[1 - \frac{(\psi-\psi_0)^2}{\Delta\psi^2}\right] \frac{B_c}{B} \frac{(1 - B/B_c)^{5/2}}{(1 - B_{\min}/B_c)^{3/2}(1 + 4B_c/B_{\min})}$$

$$\frac{1}{B}\frac{\partial P_{\perp h}}{\partial B} = -2\hat{P}_{\perp h}\left[1 - \frac{(\psi-\psi_0)^2}{\Delta\psi^2}\right] \frac{(1 - B/B_c)^{1/2}(\frac{3}{4}B^2 + BB_c + 2B_c^2)}{B_c B^3 (1 - B_{\min}/B_c)^{3/2}(1 + 4B_c/B_{\min})}$$

$$\frac{1}{B}\frac{\partial P_{\| h}}{\partial B} = -2\hat{P}_{\perp h}\left[1 - \frac{(\psi-\psi_0)^2}{\Delta\psi^2}\right] \frac{B_c}{B^3} \frac{(1 - B/B_c)^{3/2}(1 + \frac{3}{2}B/B_c)}{(1 - B_{\min}/B_c)^{3/2}(1 + 4B_c/B_{\min})}.$$

The core pressure is assumed to be constant along a field line with the radial dependence written as

$$P_c(\psi) = \begin{cases} \hat{P}_c\left[1 - \frac{(\psi-\psi_0)^2}{\Delta\psi^2}\right] & \psi > \psi_0 \\ \hat{P}_c & \psi < \psi_0. \end{cases}$$

Finally, we express the vacuum magnetic field as a function of s in the form

$$B_v(s) = B_{v\max}\left[(1 - 2\epsilon) + \epsilon\left(1 - \cos\frac{2\pi s}{L}\right)\right]. \tag{7}$$

If $\mathbf{r}(s)$ describes the position vector of a point on a field line, the curvature is given by $\boldsymbol{\kappa} = d^2\mathbf{r}/ds^2$. In a cylindrically symmetric geometry, (r, θ, z), this becomes

$\boldsymbol{\kappa} = d^2r/ds^2\hat{r} + d^2z/ds^2\hat{z}$. We will assume a long-thin system, $r/L << 1$, and note that $z = s + \mathcal{O}(r/L)^2$. So, it is reasonable to take

$$|\boldsymbol{\kappa}| \cong \frac{d^2r}{ds^2}. \tag{8}$$

Furthermore, the long-thin equilibrium condition can be written as

$$B^2(s) = B_v^2(s) - 2[P_{\perp h}(s) + P_c].$$

This implies that the finite pressure equilibrium does not change the curvature much from its vacuum value. Then, the magnetic flux is given by

$$\psi = \frac{B_v r^2}{2} + \mathcal{O}(\beta_h \Delta\psi).$$

By conservation of flux along a field line, we can then infer that

$$r^2(s) \cong r_0^2 B_{v\,\min}/B_v(s), \tag{9}$$

where $r_0 = r(s=0)$ and $B_{v\,\min} = B_v(s=0)$. Thus, Eqs. 7, 8 and 9 yield

$$\frac{\kappa}{r} \cong -\frac{\epsilon 4\pi^2}{2L^2(1-2\epsilon)}\left(\frac{r}{r_0}\right)^2\left[\cos\frac{2\pi s}{L} - \frac{3}{2}\frac{\epsilon}{1-2\epsilon}\left(\frac{r}{r_0}\right)^2\sin^2\frac{2\pi s}{L}\right]. \tag{10}$$

Using perpendicular pressure balance, these quantities give a value for the radial gradient of the field strength,

$$\frac{dB}{d\psi} = \frac{-\frac{1}{B}\frac{\partial P_{\perp h}}{\partial\psi}\Big|_B - \frac{1}{B}\frac{\partial P_c}{\partial\psi}\Big|_B + \frac{\kappa}{r}\left(1 + \frac{P_{\perp h} - P_{\| h}}{B^2}\right)}{1 + \frac{1}{B}\frac{\partial P_{\perp h}}{\partial B}\Big|_\psi}.$$

Finally, the expression for $k_\perp^2$ given below Eq. (1) can now be written as

$$k_\perp^2(s) = \frac{\ell^2}{r_0^2}\frac{B_v(s)}{B_{v\,\min}} + r_0^2 B_{\min}^2\left(\frac{\partial S}{\partial\psi}\right)^2\frac{B^2(s)}{B_{\min}^2}\frac{B_{v\,\min}}{B_v(s)} \cong k_{\perp 0}^2\frac{B^2(s)}{B_{\min}^2}\frac{B_{v\,\min}}{B_v(s)},$$

when $(r_0^4/\ell^2)(\partial S/\partial\psi)^2 B_{\min}^2 >> 1$.

Normalizing the frequency, we can write the matrix elements of Eq. (5) as

$$Q_{ij}(y) = Q_{ij}^{(a)}(y) + Q_{ij}^{(b)}(y), \tag{11}$$

$$Q_{ij}^{(a)} = \int_0^{L/2} \frac{ds}{B}\left[1+\beta_c - y^2\left(\frac{\omega_{\kappa h0}^2}{k_{\perp 0}^2 v_A^2(0)}\right)\left(\frac{B_{\min}}{B(s)}\right)^4 \frac{B_v(s)}{B_{v\,\min}} + \frac{1}{B}\frac{\partial P_{\perp h}}{\partial B}\Big|_\psi\right] f_i(s) f_j(s) \quad (11a)$$

$$Q_{ij}^{(b)} = \alpha \int_1^{B_c/B_{\min}} d\lambda\ \lambda^2 \langle f_i\rangle\langle f_j\rangle \Bigg\{(\lambda-1)\left[\frac{2(\psi-\psi_0)}{\Delta\psi} + \frac{y\left(1-\frac{(\psi-\psi_0)^2}{\Delta\psi^2}\right)\Delta_r}{R_0}\right] I^{(2)}(y,\lambda)$$
$$+ \frac{y\left(1-\frac{(\psi-\psi_0)^2}{\Delta\psi^2}\right)\Delta_r}{R_0} I^{(1)}(y,\lambda)\Bigg\}, \quad (11b)$$

with

$$I^{(1)}(y,\lambda) = \int_0^\infty \frac{dz z^{5/2} e^{-z}}{\Omega(y,\lambda,z)} = -\frac{\sqrt{\pi}}{c_1}\left[\frac{3}{4} + \frac{a}{2} + a^2 + a^{5/2}\cdot Z(a^{1/2})\right]$$

$$I^{(2)}(y,\lambda) = \int_0^\infty \frac{dz z^{7/2} e^{-z}}{\Omega(y,\lambda,z)} = -\frac{15\sqrt{\pi}}{8c_1} + aI^{(1)}(y,\lambda),$$

where we define

$$a = c_2/c_1$$

$$c_2 = \frac{\tau(\lambda) y \Delta_r}{R_0}$$

$$c_1 = \frac{\Delta\psi}{B_c}\left[\lambda\left\langle \frac{1}{r}\frac{d^2 r}{ds^2}\left(1+\frac{P_{\perp h}-P_{\|h}}{B^2}\right)\right\rangle + 2\left\langle \frac{1}{r}\frac{d^2 r}{ds^2}\left(\frac{B_c}{B}-\lambda\right)\right\rangle - \lambda\left\langle \frac{1}{B}\frac{dP_{\perp h}}{d\psi} + \frac{1}{B}\frac{dP_c}{d\psi}\right\rangle\right]$$

$$\langle\alpha\rangle = \frac{1}{\sqrt{2}}\int_0^{s_T} \frac{ds\alpha(s)}{\sqrt{1-\lambda B/B_c}}$$

$$B(s_T) = \lambda B_c$$

$$\tau(\lambda) = \langle 1\rangle$$

$$\Omega(y,\lambda,z) = c_2 - z c_1$$

$$\alpha = 2\sqrt{\frac{2}{\pi}}\frac{\hat{P}_{\perp h}}{B_c^3\left(1-\frac{B_{\min}}{B_c}\right)^{3/2}\left(1+\frac{4B_c}{B_{\min}}\right)}$$

$$\lambda = \mu B_c/\epsilon$$

$$z = \epsilon/T$$

$$y = \omega/\omega_{\kappa h0}$$

$$\omega_{\kappa h0} = \frac{\ell T}{r_0 R_0 \omega_{c\,\min}}$$

$$\omega_{c\,\min} = \frac{q_h B_{v\,\min}}{m_h}$$

$$\Delta_r = \frac{\Delta\psi}{B_{v\,\min} r_0},$$

and R_0 is the radius of curvature at $s = 0$, $R_0 = -[\kappa(s=0)]^{-1}$.

Once y is determined, the eigenfunctions can be found by fixing one of the coefficients and inverting the non-vanishing matrix to obtain the a_n's. Note that the sign of $a^{1/2}$ appearing in the integrals $I^{(1)}$ and $I^{(2)}$ is set such that its imaginary part is non-negative when $\mathrm{Im}\omega \geq 0$; this is in keeping with the definition of the plasma dispersion function used in obtaining the above expressions.

III. Results

Relevant values of the dimensionless quantities needed here are calculated using EBT-S parameters.[8] We take $B_{v\,\min} = 5kG$ (at the annulus location), and $B_{v\,\max} = 10kG$ to get a mirror ratio of 2. This corresponds to using $\epsilon = 1/4$ in Eq. (7). The length of a mirror cell is $L \sim 40$cm., and the radius of the hot electron ring is $r_0 \sim 10$cm; thus, $r_0/L = 1/4$. We can then calculate $R_0 = 16$cm. from Eq. (10). Assuming $\hat{P}_{\perp h}/B^2_{v\,\min} = .2$ yields a maximum $\beta_h \sim 40\%$. The hot electron ring is presumed to extend halfway from midplane to the mirror throat, i.e., $s_c/L = 1/4$. In determining a value for $\omega^2_{\kappa h0}/k^2_{\perp 0} v^2_A(0)$, the azimuthal and radial mode numbers must be fixed. Following Ref. 2, we assume $k^2_{\perp 0} r^2_0 = 400$ (corresponding to $k_{\perp 0} = 2/\Delta_r$ at $\Delta_r = 1$cm.). The hot electron temperature, T, is set equal to 500keV. We will consider:

$$\text{(i)} \quad \frac{\omega^2_{\kappa h0}}{k^2_{\perp 0} v^2_A(0)} = .2, \qquad \text{and} \qquad (ii) \quad \frac{\omega^2_{\kappa h0}}{k^2_{\perp 0} v^2_A(0)} = .014.$$

If we use $\ell = 3$ for the azimuthal mode number, these values correspond to core densities, $n_i = 2 \times 10^{13}\text{cm.}^{-3}$ and $1.3 \times 10^{12}\text{cm.}^{-3}$, respectively. The latter figure is typical of EBT-S experiments, while the former represents a reasonable regime for a more advanced device. Note that even if we fix $n_i = 1.3 \times 10^{12}\text{cm.}^{-3}$, we can still obtain

$$\frac{\omega^2_{\kappa h0}}{k^2_{\perp 0} v^2_A(0)} \cong .2 \qquad \text{if} \qquad \ell = 11.$$

Regardless of the interpretation of the parameters in case (i), we will see that the mode is far from marginal stability, and will give rise to some very interesting behavior when the particle drifts are reversed. Finally, we take $\psi = \psi_0 + \frac{\Delta\psi}{2}$ in order to examine the behavior of the system in the middle of the pressure gradient region.

Since Eq. (2) provides a good approximation to the eigenvalue for $\omega/\langle\omega_d\rangle << 1$, it is used to obtain a starting point for other calculations. The value of $\langle\omega_d\rangle$ can be varied by altering the annulus thickness via the parameter $\Delta_{rm} = \Delta_r/r_0$; in particular, $\omega/\langle\omega_d\rangle << 1$ when $\Delta_{rm} << 1$. Following experimental estimates, previous theoretical investigations used $\Delta_r = 1 - 2$cm. (i.e., $\Delta_{rm} = .1 - .2$); more recent measurements show that Δ_r may be as large as 5cm.[9,10,11]

Figures 1 $\left(\frac{\omega^2_{\kappa h0}}{k^2_{\perp 0} v^2_A(0)} = .2\right)$ and 2 $\left(\frac{\omega^2_{\kappa h0}}{k^2_{\perp 0} v^2_A(0)} = .014\right)$ show the imaginary part of the eigenvalue as the parameter Δ_{rm} is scanned. Both of these figures contain curves generated by using the asymptotic expansion, Eq. (2), and in each case, the results match quite well with complete solution for $\Delta_{rm} \lesssim .1$, but differ significantly for larger ring widths. The errors increase as the scan proceeds due to a gradual decrease in the validity of the expansion of the resonant denominator. Also, it is apparent that Eq. (2) yields stable solutions for greater pressure gradients than the integral equation. Thus, we see that the integral equation gives more pessimistic results.

Since $\frac{\omega^2_{\kappa h0}}{k^2_{\perp 0} v^2_A(0)}$ is proportional to n_i; the solutions of the integral equation indicate that a smaller core density will allow a larger pressure gradient before the magnetic compressional mode is destabilized. In particular, Fig. 2 suggests that $\Delta_r/r_0 \gtrsim .2$ is needed for the system to be stable. The very high density case, represented by Fig. 1, requires a considerably wider ring to be stable, $\Delta_r \gtrsim r_0/2$. There are other interesting effects occurring in this case; all of the calculations to follow assume $\frac{\omega^2_{\kappa h0}}{k^2_{\perp 0} v^2_A(0)} = .2$.

Now, we fix the value of Δ_{rm} and scan over the core pressure, $\hat{P}_c(\beta_c \sim 2\hat{P}_c/B^2_{v\,\min})$. Figure 3 shows the imaginary part of the eigenvalue for $\Delta_{rm} = .3$. In the plot, three curves appear, representing the results of using: $\hat{B}_{\|} = \frac{C(\psi)}{B}\ \frac{dP_{\perp h}}{d\psi}$, ten term cosine series, and the asymptotic expansion. All three of these methods indicate stability for $\beta_c \gtrsim 17\%$. From the results of Refs. 2, 6 and 12, it is known that the magnetic compressional mode is stable for all values of n_h/n_i if $\beta_c R_0/2\Delta_r > 1 + P_{\|h}/P_{\perp h}$. But, since we consider here one

particular nonzero value of n_h/n_i, the restriction on β_c is less severe, about half of what is required by $\frac{\beta_c R_0}{2\Delta_r} > 1$.

An analytic approach which is valid for arbitrary values of Δ_{rm} can be obtained in the manner described by Berk, et al.[2] The authors employ a delta function distribution for the hot electrons in a local (no bounce averages) WKB approximation. If we take

$$F_h(p_\parallel, \mu) \propto \delta(p_\parallel - p_{\parallel 0})\delta(\mu - \mu_0),$$

with $\beta_h \sim P_{\parallel h}/P_{\perp h} < 1$, we obtain a cubic dispersion relation for the magnetic compressional mode (we evaluate all quantities at midplane, $s = 0$)

$$y^3 + a_2 y^2 + a_1 y + a_0 = 0, \tag{12}$$

where

$$a_2 = -\frac{B_{v\,\min}}{c_0 B_{\min}}\left(r_0 R_0 \frac{dB}{d\psi} - P_{\parallel h}/P_{\perp h}\right)$$

$$a_1 = -(1 + \beta_c + \beta_{\perp h})\frac{k_{\perp 0}^2 v_A^2(0)}{\omega_{\kappa h 0}^2}$$

$$a_0 = -\frac{B_{v\,\min}}{c_0 B_{\min}}\frac{k_{\perp 0}^2 v_A^2(0)}{\omega_{\kappa h 0}^2}\left[1 + P_{\parallel h}/P_{\perp h} + R_0 r_0 B_{\min}\,\frac{d}{d\psi}\left(\frac{P_c}{B^2}\right)\right],$$

and c_0 is a numerical factor relating μ_0 to the parameter T used in Eq. (6).

It is a straightforward procedure to calculate the marginally stable value of $\hat{P}_c$ for a given value of Δ_{rm}. A calculation with the parameters used in Fig. 3 gives a value within 10% of that seen in the plot. Discrepancies of this size can then be attributed to the lack of field line averages and to differences in the distribution function. Note also that when $\frac{\beta_c R_0}{2\Delta_r}$ becomes larger than $1 + \frac{P_{\parallel h}}{P_{\perp h}}$, a_0 changes sign and forces the roots obtained by balancing the last three terms in Eq. (13) to be real for any value of $\frac{\omega_{\kappa h 0}^2}{k_{\perp 0}^2 v_A^2(0)}$. This is the origin of the criterion discussed in Refs. 2, 6 and 12.

Returning now to Fig. 3, we note that the results obtained from using $\hat{B}_\parallel = \frac{C(\psi)}{B}\,\frac{dP_{\perp h}}{d\psi}$ differ by less than 10% from those calculated with the ten term cosine series. The asymptotic expansion is considerably less accurate, as would be expected for such a large value of Δ_{rm}. However, these differences get smaller as $\hat{P}_c$ increases, becoming

negligible as marginal stability is approached. Similar behavior is observed at other values of Δ_{rm}.

Figures 4 and 5 show the field line dependence of $\hat{B}_{||}$ in two cases. This is determined by the method described in Sec. II. For comparison, we include a plot of $(1/B)dP_{\perp h}/d\psi$ as a function of s. We then see that the reason for the above trend is that $\hat{B}_{||}(s)$ converges toward $(1/B)dP_{\perp h}/d\psi(s)$ as the core pressure gets larger. Note that the single term result yields a good eigenvalue for $\frac{\hat{P}_c}{B^2_{v\,\min}} = .002$ even though the eigenfunction differs considerably from the correct result.

We note that the degree of validity of $\hat{B}_{||} = (C(\psi)/B)dP_{\perp h}/d\psi$ is dependent on the extent to which[6]

$$\left|\frac{1}{B}\frac{dP_{\perp h}}{d\psi}\right| > \left|\frac{\kappa\sigma}{r} - \frac{1}{B}\frac{dP_c}{d\psi}\right|. \tag{13}$$

Then it is clear that this approximate form of $\hat{B}_{||}$, as well as the expansion of the resonant denominator in Eq. (2), will become more accurate as the core pressure is increased. This explains the decreases in the errors seen in Figs. 3-5.

When the above inequality is well satisfied, the hot particle drifts are reversed from their vacuum values. For $\hat{P}_c = 0$, this is the case for $\Delta_{rm} \lesssim .25$. However, $\Delta_{rm} = .3$ yields drifts in the same direction as in vacuum. But, it is clear from Eq. (11) that larger core pressures may also bring about drift reversal. This occurs in Fig. 3 before the marginally stable point is reached; that is, Eq. (13) is then well satisfied.

Using the calculated coefficients, a_n, and eigenvalue, ω, both sides of Eq. (1) can be computed as a function of the number of terms in the series, N. In Fig. 6 we plot the negative logarithm of δ, defined as the absolute value of the difference between the right and left-hand sides of Eq. (1) for $N = 2 - 10$, and $\Delta_{rm} = .1$, .2, .3, and .4. This is a measure of how well the expansion worked at each N. Clearly, $N = 10$ represents an effectively converged series for $\Delta_{rm} = .1$ and 2, but not for $\Delta_{rm} = .3$ and .4. For $\Delta_{rm} > .4$, ten terms soon become insufficient to represent the eigenfunction, and we are not able to deterine the marginally stable point at large core densities using this method. The single term representation, $\hat{B}_{||} = \frac{C(\psi)}{B}\,\frac{dP_{\perp h}}{d\psi}$, also becomes ineffective at this point. For example, Fig. 7 shows the eigenfunction calculated using the ten terms with $\Delta_{rm} = .4435$

and $\hat{P}_c/B^2_{v\,\min} = .002$. The peak near $s_0 = .07$ requires a more rapid variation along the field line than f_{10} is capable of providing. As a result, there is quite a bit of overshoot at large s where $\hat{B}_{||}$ should be smoothly approaching zero.

At this point, the Gaussian test function of Eq. (4) proves very useful. The curve in Fig. 1 is extended past $\Delta_{rm} = .4$ by this approach. Matching results at $\Delta_{rm} = .4$ as closely as possible suggests setting $s_0 = .04$. We then observe that the mode stabilizes when $\Delta_{rm} \gtrsim .5$, and is damped from there on. Apparently, the change in sign of Im ω results from a change in the relative sizes of the $\omega\frac{\partial F}{\partial \epsilon}$ and $\frac{\partial F}{\partial \psi}$ terms in the kinetic integral. This behavior can be explained as follows. First, we note that Re y = Re$(\omega/\omega_{\kappa h0}) < 0$ in all cases. When the average drift frequency, $\langle\omega_d\rangle$ (a function of pitch angle, λ), is normalized in the same manner, it is positive for drift reversed particles (small Δ_{rm}). In this case, if Im $\omega = 0$, $I^{(1)}$ and $I^{(2)}$ of Eq. (11b) are real, and it is possible to have purely oscillatory solutions, as in Fig. 2 for $\Delta_{rm} \gtrsim .2$. Here, the decreases in $\frac{\partial F}{\partial \psi}$ and $\langle\omega_d\rangle$ arising from the increase in Δ_{rm} gradually reduce the effect of the hot electrons, and, hence, lower the growth rate.

However, $\langle\omega_d\rangle < 0$ for large Δ_{rm}, and there is a possibility of having particles resonate with the wave, Re $\omega = \langle\omega_d\rangle$. Due to the fact that all particle energies are allowed by the chosen hot electron distribution function, there is always a fraction of particles for which this is approximately true, and for this reason, there is always some imaginary contribution made by $I^{(1)}$ and $I^{(2)}$. To obtain marginal stability now, the $\frac{\partial F}{\partial \psi}$ term must be small enough to exactly cancel $\omega\,\frac{\partial F}{\partial \epsilon}$ in the kinetic integral, e.g., for $\Delta_{rm} \gtrsim .5$ in Fig. 1. Unlike the case in Fig. 2, the solutions at larger Δ_{rm} are not oscillatory, but damped.

The peak observed in Figs. 4 and 7 is a characteristic of the resonance. Apparently, the eigenfunction reaches a maximum value at a position along the field line near the turning point, $s_T(\lambda)$, of the pitch angle, λ, which yields the average drift, $\langle\omega_d\rangle_\lambda$, closest to being resonant with the wave frequency, ω. As Im ω decreases, the peak becomes more pronounced. Thus, we expect the convergence of the cosine series to get worse as the mode stabilizes. The Gaussian test function was chosen to circumvent this problem and appears to do so effectively. As was mentioned before, increasing the core pressure towards marginal stability for $\Delta_{rm} = .3$ and .4 also gives rise to drift reversal. In that case, the

resonance is removed, and convergence should improve.

IV. Summary

We have numerically solved the integral equation to determine the eigenvalues and eigenfunctions of the magnetic compressional mode; the results match those of the asymptotic expansion in the case of a deep diamagnetic well. The use of a trial function, $\hat{B}_{\|} = \frac{C(\psi)}{B} \frac{dP_{\perp h}}{d\psi}$ is found to give accurate eigenvalues over a large range of parameter values (Fig. 3), although $\frac{C(\psi)}{B} \frac{dP_{\perp h}}{d\psi}$ can at times differ considerably from the actual $\hat{B}_{\|}$ (Fig. 4).

In those cases where there is no drift reversal, and large core densities are present, a wave-particle resonance appears and causes the mode to be unstable unless the ring half-width is some significant fraction of the annulus radius. Numerically, it has the effect of reducing the rate of convergence of the expansion, Eq. (3) (Fig. 6); eventually, it makes solutions via that method impractical. Use of the Gaussian test function, Eq. (4), proves very helpful in following the mode to marginal stability in this case.

Small values of the ring half-width, $\Delta_r \lesssim$ 2cm., indicate instability for values of the core density, n_i (Fig. 2) achieved experimentally. The real part of the frequency near marginal stability is on the order of the curvature drift frequency of the hot electrons: $\omega \sim 2\omega_{\kappa h0}$ in Fig. 1, and $\omega \sim 4\omega_{\kappa h0}$ in Fig. 2. With the parameters used in Sec. III, we can calculate corresponding oscillation frequencies, $\frac{\omega}{2\pi} \sim$ 60 and 120 MHz, respectively, Hiroe. et al.[13] recently reported experimental observations of instabilities with frequencies around 100 MHz as the ambient pressure was reduced from the T-mode regime; further reductions of the ambient pressure were accompanied by a drop in this frequency, peaking near 20 MHz at the T-M transition. Although the magnetic compressional mode cannot be clearly identified as the source of these fluctuations, it should not be ruled out as a possible source.

Recent experimental determinations of radial width indicate that the radial scale lengths are considerbly larger than 2cm. in EBT-S.[9,10,11] On face value, this would indicate that the magnetic compressional mode should not be excited. However, it is still a possibility that the nonlinear properties of the mode are causing the observed radial

spreading of what would otherwise be a sharp distribution.

Finally, an analytic approach employing a delta function distribution for the hot electron,[2,6] is used to provide values of the core pressure and density at marginal stability. The results of the calculations are in good agreement with the numerical computations in the drift reversed situations. The condition for stability of the magnetic compressional mode with an arbitrary value of n_h/n_i then appears to be that $\beta_c R/2\Delta_r > 1 + P_{\|h}/P_{\perp h}$, even when $\beta_h R/2\Delta_r$ is not large. Of course, if this were the case, more familiar MHD modes could be unstable. In particular, note that this criterion requires a value of β_c above the Lee-Van Dam limit for stability of the interacting pressure-driven interchange. More generally, it is seen that a given value of n_h/n_i can be stable if the pressure scale length, Δ_r, is large enough.

References

1. M.N. Rosenbluth, Phys. Rev. Lett. **46**, 1525 (1981).
2. H.L. Berk, J.W. Van Dam, M.N. Rosenbluth, and D.A. Spong, Phys. Fluids **26**, 201 (1983).
3. A.M. El Nadi, Phys. Fluids **25**, 2019 (1982).
4. D.E. Baldwin and H.L. Berk, Phys. Fluids **26**, 3595 (1984).
5. H.L. Berk and H.V. Wong, Phys. Fluids **28**, 1881 (1985).
6. H.L. Berk, C.Z. Cheng, M.N. Rosenbluth, and J.W. Van Dam, Phys. Fluids **26**, 2642 (1983).
7. T.M. Antonsen, Jr. and Y.C. Lee, Phys. Fluids **25**, 132 (1982).
8. R.J. Colchin, T. Uckan, F.W. Baity, L.A. Berry, F.M. Bieniosek, L. Bighel, W.A. Davis, E. Dullni, H.O. Eason, J.C. Glowienka, G.A. Hallock, G.R. Haste, D.L. Hillis, A. Komori, T.L. Owens, R.K. Richards, L. Solensen, T.L. White, and J.B. Wilgen, Plasma Phys. **25**, 597 (1983).
9. D.L. Hillis, J.B. Wilgen, J.A. Cobble, W.A. Davis, S. Hiroe, D.A. Rasmussen, R.K. Richards, T. Uckan, E.F. Jaeger, O.E. Hankins, J.R. Goyer, and L. Solensten, Phys. Fluids **28**, 2848 (1985).
10. D.L. Hillis, J.B. Wilgen, S.T. Bigelow, E.F. Jaeger, D.W. Swain, O.E. Hankins, and R.E. Juhuala, submitted to Phys. Fluids.
11. E.F. Jaeger, L.A. Berry, C.L. Hedrick, and R.K. Richards, Nucl. Fusion **25**, 71 (1985).
12. D.A. Spong, H.L. Berk, and J.W. Van Dam, Phys. Fluids **26**, 2652 (1983).
13. S. Hiroe, J.B. Wilgen, F.W. Baity, L.A. Berry, R.J. Colchin, W.A. Davis, A.M. El Nadi, G.R. Haste, D.L. Hillis, D.A. Spong, T. Uckan, and T.L. Owens, Phys. Fluids **27**, 1019 (1984).

Figures Captions

1. Imaginary part of the eigenvalue plotted as a function of the parameter Δ_{rm} with $\omega_{\kappa h0}^2/k_{\perp 0}^2 v_A^2(0) = .2$. Curves representing a calculation with a ten term series expansion for $\hat{B}_{||}$, and one with the asymptotic expansion, Eq. (2), and a Gaussian test function (Eq. (4), with $s_0 = .04$), appear.
2. Imaginary part of the eigenvalue plotted as a function of the parameter Δ_{rm} with $\omega_{\kappa h0}^2/k_{\perp 0}^2 v_A^2(0) = .014$. Curves representing a calculation with a seven term series expansion for $\hat{B}_{||}$, and one with the asymptotic expansion, Eq. (2), appear.
3. Imaginary part of the eigenvalue plotted as a function of the parameter, $\frac{\hat{P}_c}{B_{v\,\min}^2}$ with $\Delta_{rm} = .3$. Three curves appear: one term representation, $\hat{B}_{||} = (C(\psi)/B)dP_{\perp h}/d\psi$; ten term cosine series; and the asymptotic expansion, Eq. (2).
4. Eigenfunction plotted as a function of the distance along the field line, s, for $\Delta_{rm} = .3$ and $\frac{\hat{P}_c}{B_{v\,\min}^2} = .002$. Two curves appear; one is the result of the ten term cosine series calculation; the other is a plot of $(1/B)dP_{\perp h}/d\psi$ provided for comparison.
5. Eigenfunction plotted as a function of the distance along the field line, s, for $\Delta_{rm} = .3$ and $\frac{\hat{P}_c}{B_{v\,\min}^2} = .084$. Two curves appear; one is the result of the ten term cosine series calculation; the other is a plot of $(1/B)dP_{\perp h}/d\psi$ provided for comparison.
6. Negative logarithm of δ, the difference between right and left-hand sides of Eq. (1), evaluated with the values of ω and $\hat{B}_{||}$ obtained by using an N term cosine series expression for $\hat{B}_{||}$. Separate curves appear for $\Delta_{rm} = .1, .2, .3$ and $.4$.
7. Eigenfunction plotted as a function of the distance along the field line, s, for $\Delta_{rm} = .4435$ and $\frac{\hat{P}_c}{B_{v\,\min}^2} = .002$. The ten term cosine series is used in the calculation.

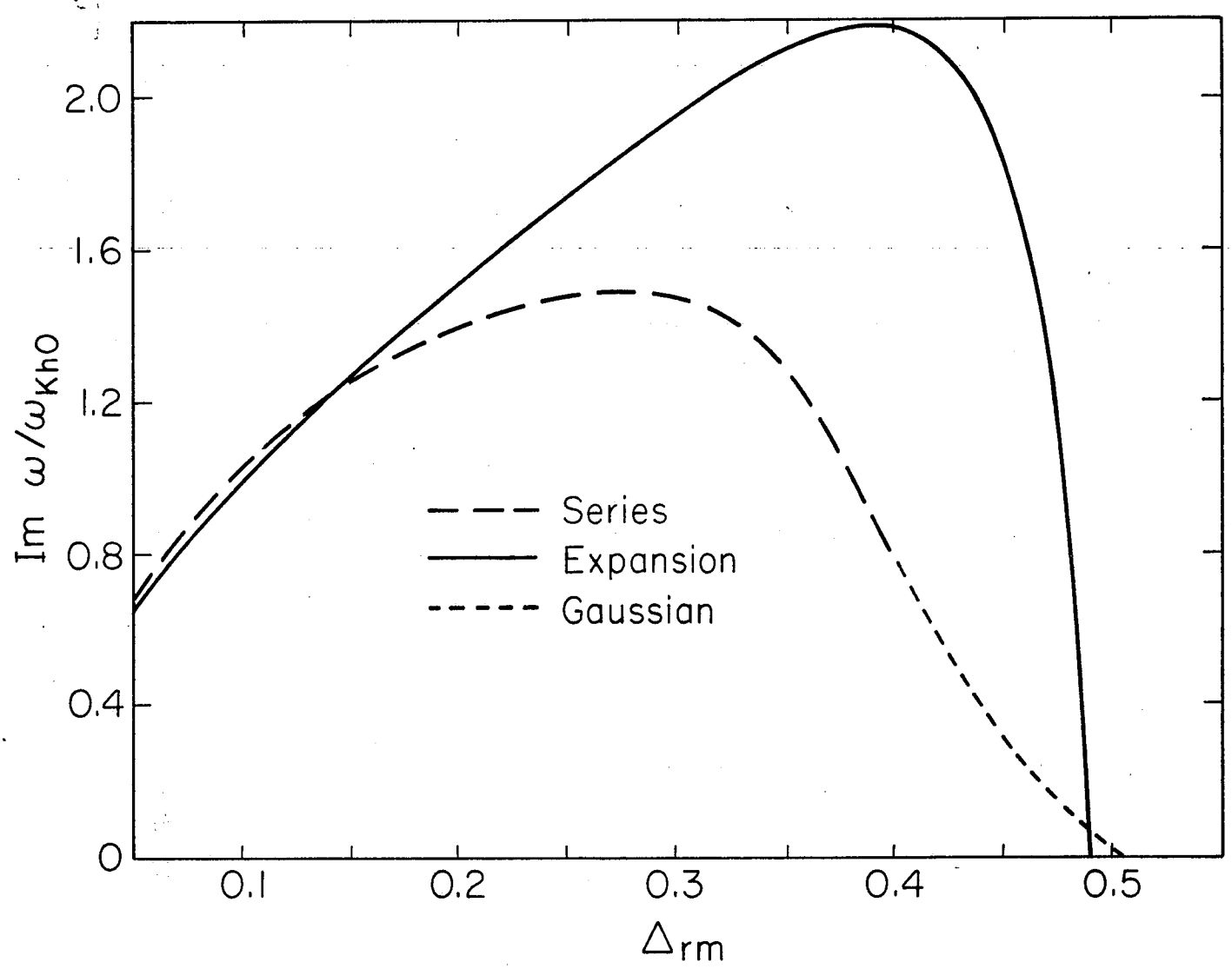
2.0
1.6
1.2
0.8
0.4
0
Im ω/ω_Kh0
0.1
0.2
0.3
0.4
0.5
Δrm
Series
Expansion
Gaussian

Fig. 1

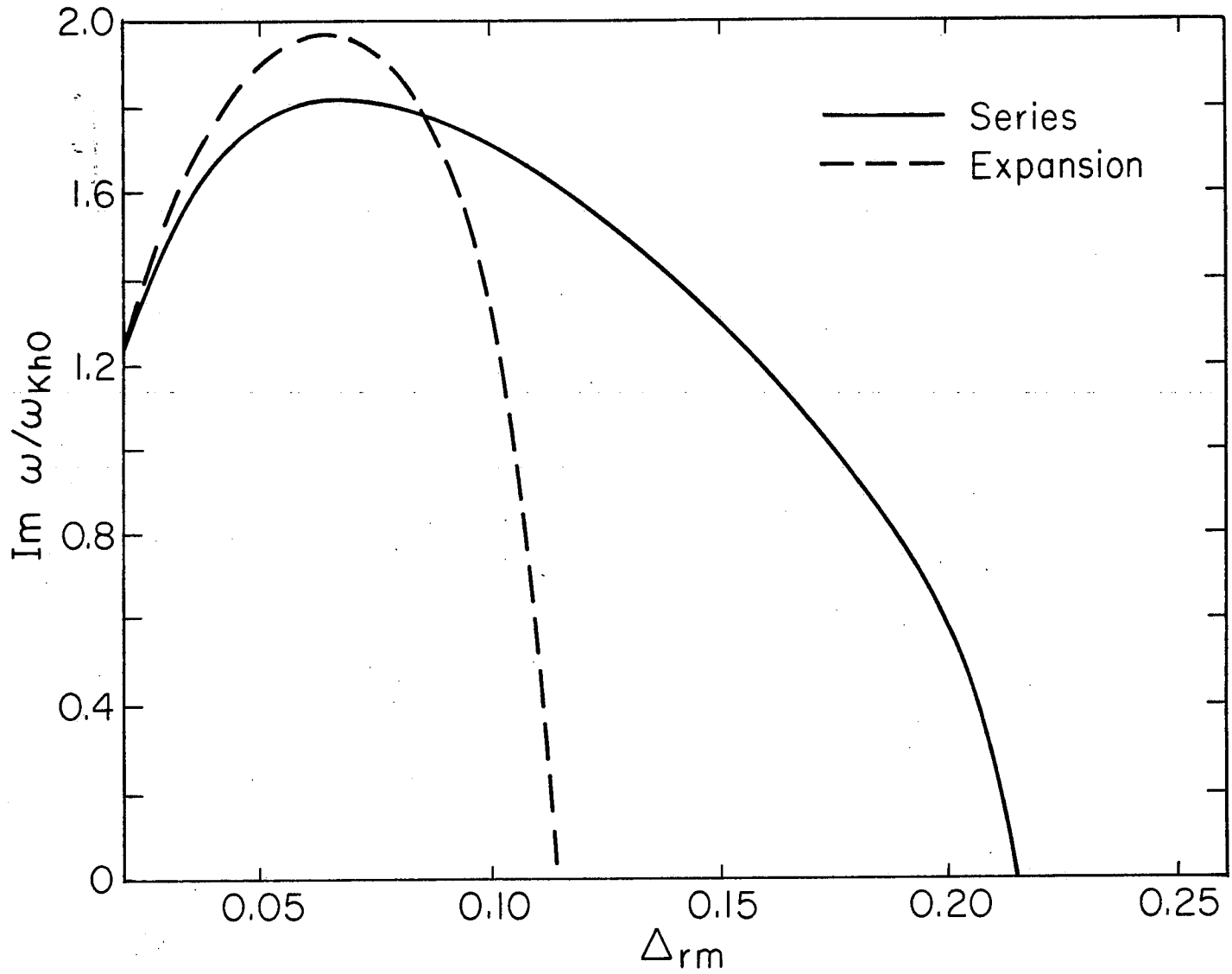
2.0
1.6
1.2
0.8
0.4
0
Im ω/ω_KHO
0.05
0.10
0.15
0.20
0.25
Δ_rm
Series
Expansion

Fig. 2

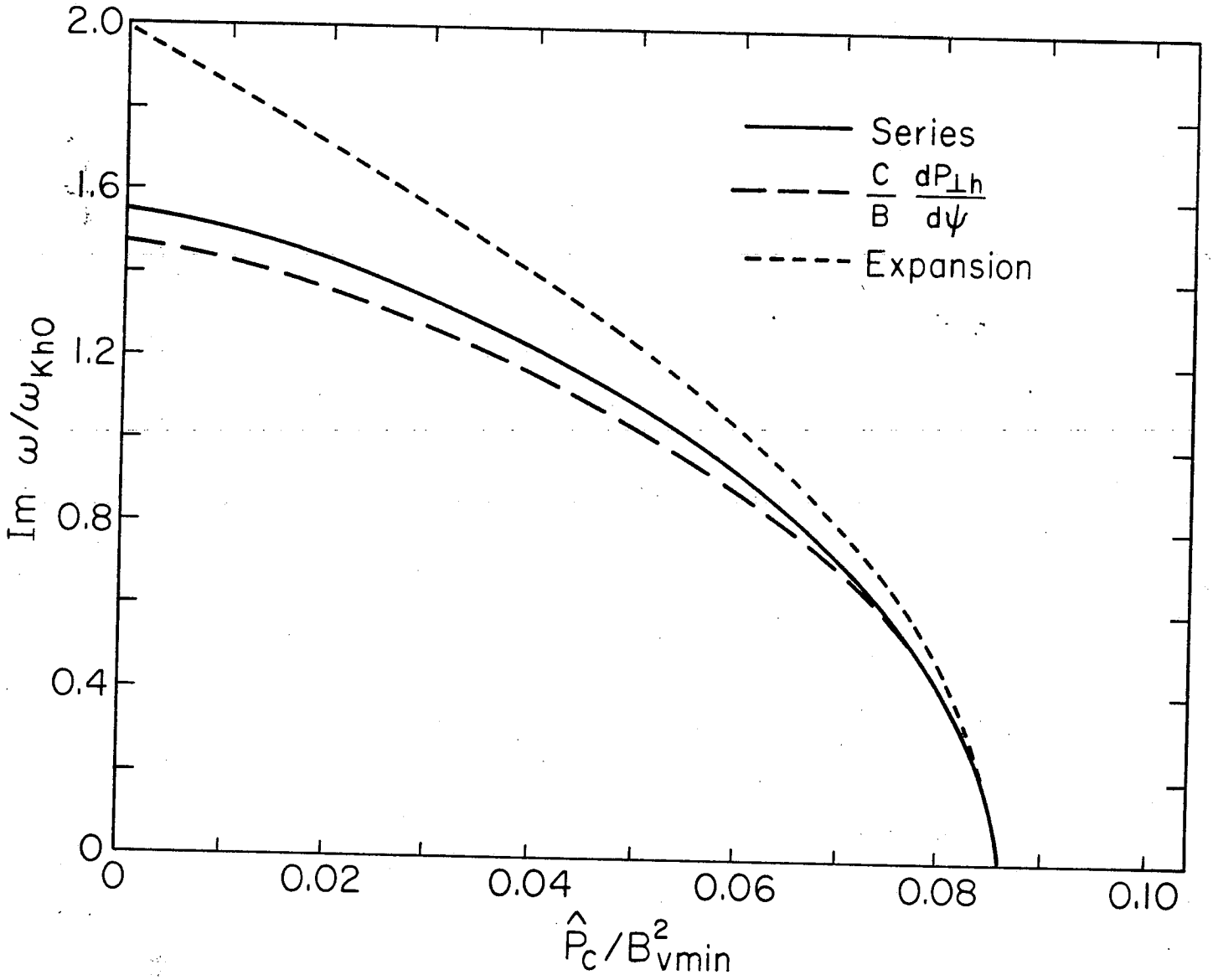
2.0
1.6
1.2
0.8
0.4
0
Im ω/ω_{Kh0}
0
0.02
0.04
0.06
0.08
0.10
$\hat{P}_c/B^2_{vmin}$
Series
$\frac{C}{B}\frac{dP_{\perp h}}{d\psi}$
Expansion

Fig. 3

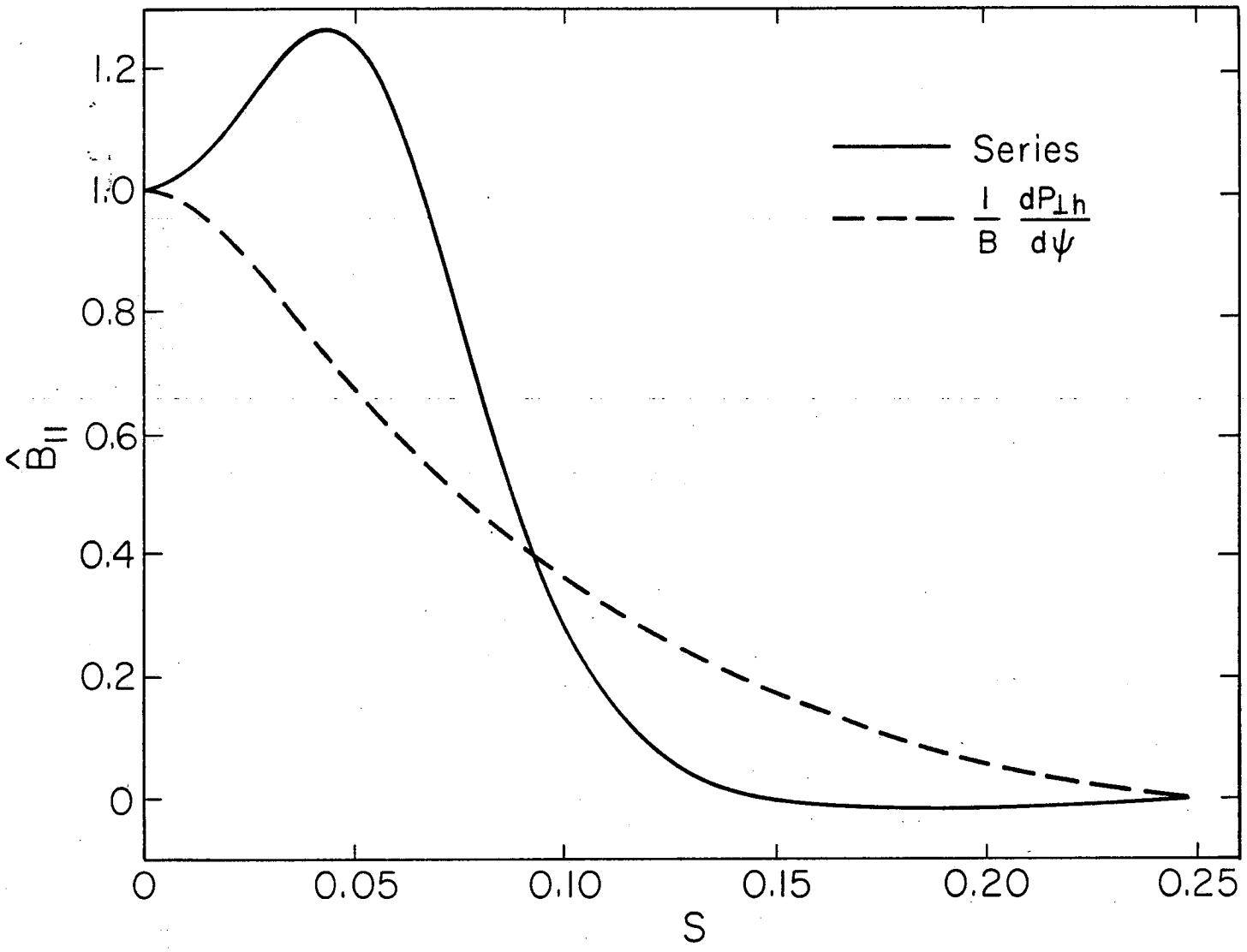
1.2
1.0
0.8
0.6
0.4
0.2
0
$\langle B_{\parallel} \rangle$
0
0.05
0.10
0.15
0.20
0.25
S
Series
$\frac{1}{B} \frac{dP_{\perp h}}{d\psi}$

Fig. 4

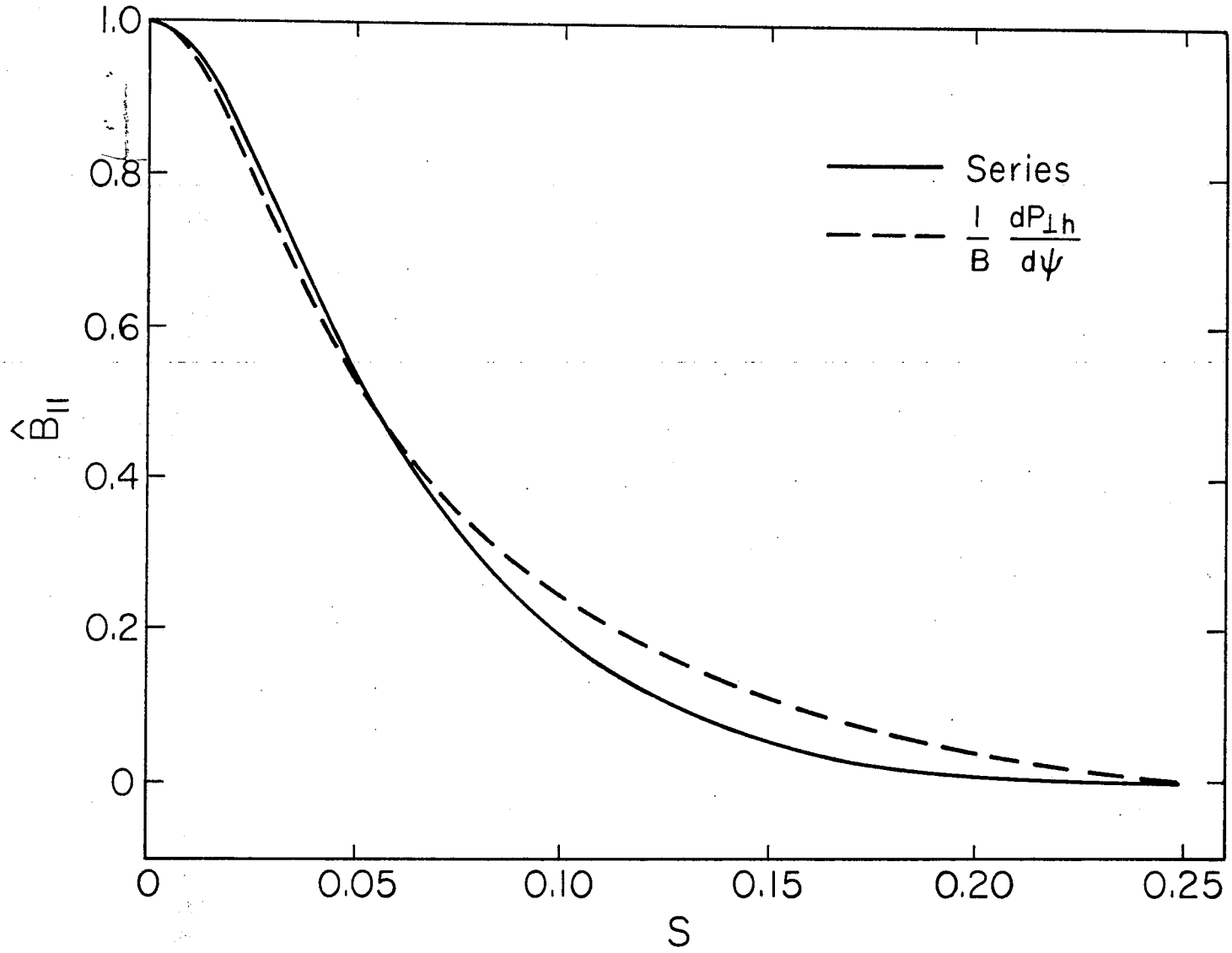

Fig. 5

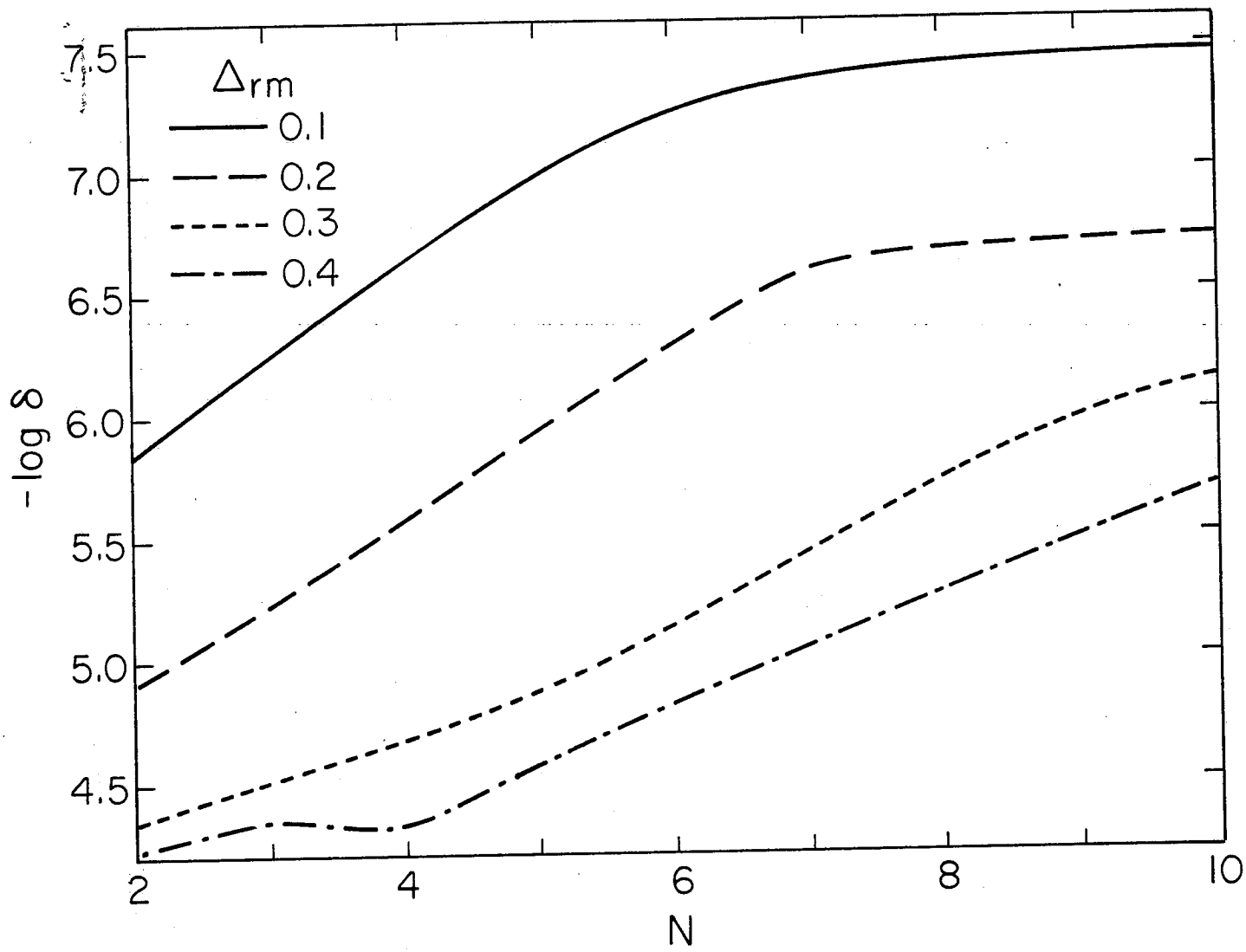

Fig. 6

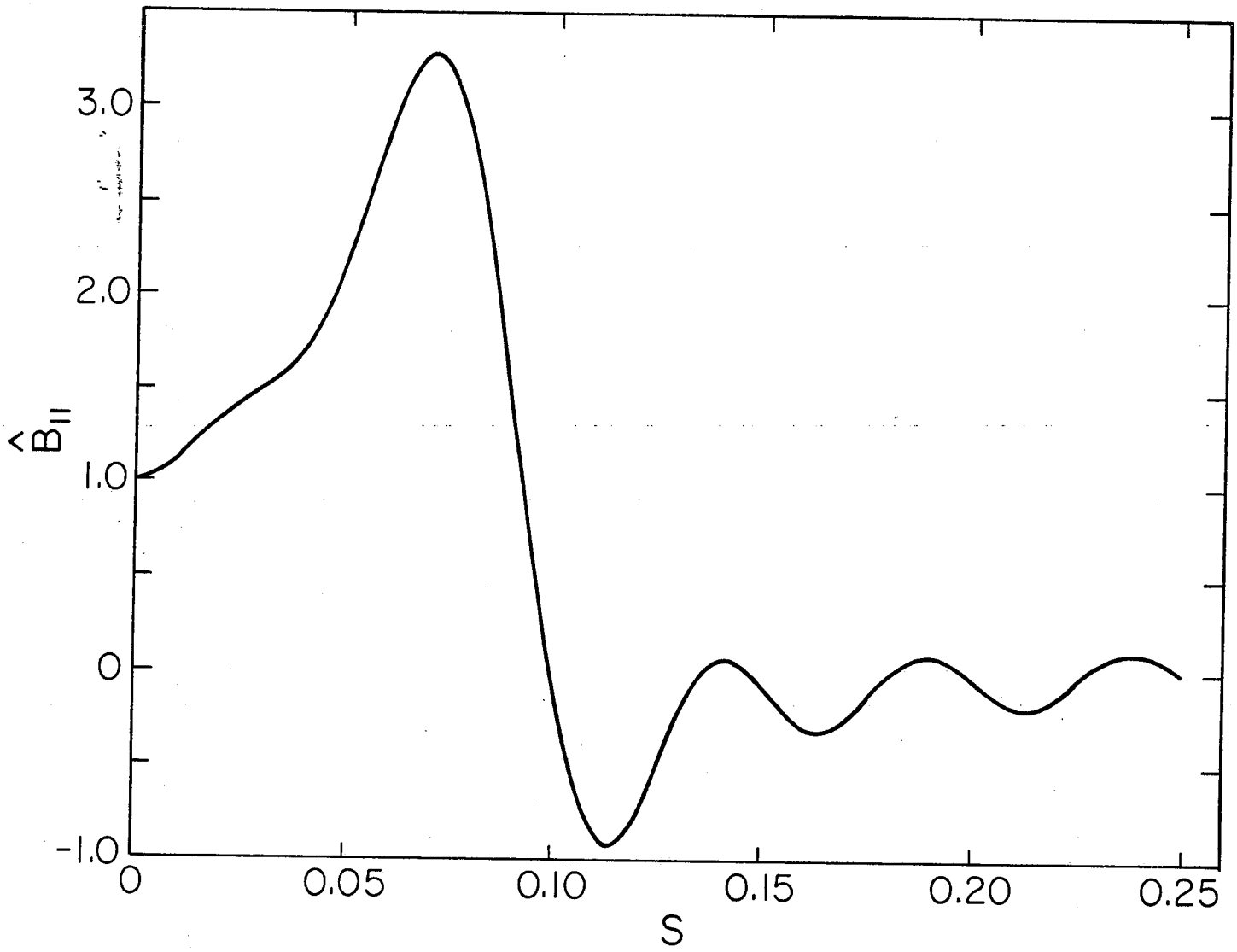

Fig. 7